

Surface Finishing and Shape Effects on Corrosion Resistance of Ti-6Al-4V Alloy in the Simulated Body Fluid

R.C. Souza^{a,*} , C.A.R. Maestro^a, S.L.M. Ribeiro Filho^{a,c}, S. Clemasco^a, B.A.F. Santos^a ,
M.E.D. Serenário^a, A.M. De Sousa Malafaia^a , I.N. Bastos^b , L.C. Brandão^a , A.H.S. Bueno^a 

^aUniversidade Federal de São João Del-Rei (UFSJ), Departamento de Engenharia Mecânica e Industrial, Campus Santo Antônio, Praça Frei Orlando, 170, Centro, 36307-352, São João Del Rei, MG, Brasil.

^bUniversidade do Estado do Rio de Janeiro (UERJ), Instituto Politécnico (IPRJ), Rua Bonfim, 25, 28625-570, Nova Friburgo, RJ, Brasil.

^cInstituto Tecnológico de Aeronáutica, Divisão de Engenharia Aeronáutica e Mecânica, São José dos Campos, SP, Brasil.

Received: October 20, 2021; Revised: June 01, 2022; Accepted: June 05, 2022

Pure titanium and various alloys, such as Ti-6Al-4V, are widely used as biomaterials. In this application, surface finish conditions, topography, and surface reactivity determine excellent cellular adhesion and osseointegration characteristics. The study evaluated the influence of four surface finishing treatments (sanding #120, 600, 1200, and polished with 3 μm alumina paste) and three shapes (concave, convex, and flat) on the corrosion resistance of Ti-6Al-4V at 37 °C in simulated body fluid (SBF) through potentiodynamic polarization and electrochemical impedance spectroscopy. The SBF's ionic composition allowed the formation of a stable passive layer with a low presence of pores on the surface. In addition, the combination of polished surface and convex shape showed the best electrochemical passive behavior.

Keywords: *Ti-6Al-4V alloy, Surface finishing, Shape, Simulated body fluid.*

1. Introduction

Biomaterials is often necessary to reconstruct or replace structures like bone and cartilaginous tissue damaged by internal or external diseases or traumas. As much as biomaterials are considered inert, they cause biological responses related to success in the post-implantation period. Simultaneously, the organism can cause wear or corrosion at the implanted material^{1,2}. Thus, it is expected that a biomaterial has good mechanical properties, osseointegration, and high resistance to corrosion and wear, in addition to being non-toxic and not causing rejection by the adjacent tissue²⁻⁴.

Titanium and its alloys are one of the most widely used metallic materials as biomaterials. The reasons are its relatively low specific mass and low elastic modulus, high corrosion resistance, inertness in the body environment, high biocompatibility, and excellent interaction with body tissues⁵⁻⁷. This high biocompatibility is related to a TiO₂ passive film that spontaneously forms on the metallic surface when exposed to air. Moreover, if the film breaks and exposes the bare material to a corrosive environment, it can be quickly repassivated³. Titanium and its alloys can be classified, regarding their microstructures, as α , near- α , ($\alpha + \beta$), and β . For example, Ti-6Al-4V is the most widely used titanium alloy in bioapplications and has the structure $\alpha + \beta$, where the alpha phase is stabilized by the aluminum and the beta phase by the vanadium⁸.

Despite its wide application as a biomaterial, the localized corrosion such as pit is the main responsible for the compromised biocompatibility of the Ti-6Al-4V alloy⁹. Once corrosion of the material occurs, toxic aluminum or vanadium ions can be released, causing inflammation that can loosen the implant or even trigger neurological diseases^{6,10-12}. The pits are characterized by a localized occurrence and are challenging to predict, as they require a long period of initialization¹³. Besides directly influencing the mechanical properties, the material's surface finish is related to the material's corrosion resistance. The polarization curves obtained by Cheng and Roscoe¹⁴ for the different surface roughness of commercially pure titanium show that for potential below 1.7 V (SCE), the current density decreases with the reduction of surface roughness, i.e., the corrosion resistance increases with roughness decrease. It is worth mentioning that these results may vary according to the solution used since the solution's ionic composition also influences the formation of the passive protective layer.

Another essential characteristic of the implants is their shape. Several shapes are found regarding implants that can be flat, circular, screw thread, concave, and convex⁶, being an important characteristic during materials selection for medical devices products¹⁵. Geometric characteristics, such as concave and convex, can be related to different layer formations in metallic materials, as was observed by the galvanized steel studied by McMurray et al.¹⁶. The shape also

* e-mail: rhuaneufsj@gmail.com

influences the titanium passivation mechanisms, as detailed by Gai et al.¹⁷. The authors reported that for different shapes, the mass transport of dissolved oxygen is faster in convex surfaces than in concave ones. Moreover, the shape of parts produced by machining alters the surface residual stress that affects the film of passive alloys. Furthermore, related to biological response, it was demonstrated that concave surfaces are better for cell growth and tissue regeneration than convex and flat surfaces¹⁸.

Considering the importance of surface finishing and geometric shapes on biomaterials area and the lack of studies evaluating corrosion response in concave and convex surfaces, the purpose of this study was to evaluate the influence of these characteristics on the corrosion resistance of Ti-6Al-4V alloy at 37 °C in simulated body fluid. The samples were prepared with four surface finishes, obtained by sanding/polishing, and three shapes obtained by milling. The electrochemical characteristics were evaluated by potentiodynamic polarization and impedance tests.

2. Methodology

2.1. Materials and metallographic characterization

Square-shaped samples of Ti-6Al-4V, with 15 mm sides and an exposed area of approximately 2.3 cm² were used for microstructural characterization and electrochemical corrosion tests. First, the solubilized sample was sanded using SiC papers (until #1200) and polished with 3 μm alumina paste for surface characterization. Then, the samples were cleaned with isopropyl alcohol and distilled water under ultrasound stirring for 3 minutes. Subsequently, the samples were dried and etched for 5 seconds at room temperature by immersion in a solution containing 2% hydrofluoric acid (HF) and 10% nitrite acid (HNO₃) to reveal the microstructure. After the etching, the sample was characterized by optical microscopy using an Olympus microscope, model BX51, and x-ray diffraction (XRD) using Cu-Kα radiation and 2θ-angle scanning from 20 to 80°.

The samples were divided into two groups regarding surface finishing and surface shape for the polarization and impedance electrochemical tests. First, a group aimed to evaluate the influence of surface finishing treatments on the material's corrosion resistance. Thus, the sample's surfaces were prepared in four conditions: sanded, using SiC papers up to 120, 600, #1200, and polished with 3 μm alumina paste.

The objective of the other group was to evaluate the influence of the sample shape on corrosion resistance. The samples were milled in Romi Discovery 560 vertical machining center with a 40 m/min cutting speed and a 0.05 mm/rot feed. These parameters were kept constant, and three surfaces were generated: flat, concave, and convex. Figure 1 shows the schematic drawings of the shape profiles generated. After milling, the samples were polished with SiC sandpaper (#500) to standardize the surface finish. For both groups, the samples were electrochemically tested immediately after surface preparation.

2.3. Electrochemical tests

Potentiodynamic polarization tests were used to analyze the current density from the potential scanning, based on the ASTM G5-94 standard¹⁹. The tests were performed in an Autolab Multi Potentiostat model PGSTAT101, using a flat cell with a platinum net as a counter-electrode, a saturated calomel reference-electrode (SCE), and the titanium alloy as the working-electrode. The potential scan rate was 0.33 mV/s. The electrolyte was the simulated body fluid (SBF) maintained at 37 °C. The solution was produced according to the reference²⁰, and its composition is shown in Table 1. The current density is expressed by the parameter *j*.

The electrochemical impedance spectroscopy (EIS) was performed in the same cell described for the polarization test, with SBF solution at 37 °C. Initially, the samples were kept in solution for 3600 seconds, and then the corrosion potential (*E*_{corr}) was determined. The analyses were performed at the corrosion potential with a frequency scanning range from 100 kHz to 10 mHz and an rms voltage perturbation of

Table 1. Chemical composition necessary to prepare 1000 mL of simulated body fluid (SBF). Adapted from²⁰.

Addition sequence	Chemical	Quantity (g)	Purity (%)
1	NaCl	8.035	99.5
2	NaHCO ₃	0.355	99.5
3	KCl	0.255	99.5
4	K ₂ HPO ₄ ·3H ₂ O	0.231	99.0
5	MgCl ₂ ·6H ₂ O	0.311	98.0
6	HCl (1.0 mol/L)	39.0 mL	----
7	CaCl ₂	0.292	95.0
8	Na ₂ SO ₄	0.072	99.0
9	(CH ₂ OH) ₃ CNH ₂	6.118	99.0

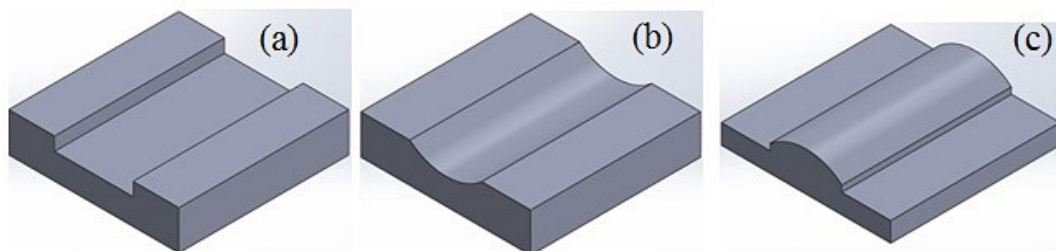


Figure 1. Surface shape obtained by milling: a) flat, b) concave, c) convex.

10 mV. All electrochemical tests were performed in triplicate. The potential was referred to SCE. The electrochemical impedance diagrams were fitted by the equivalent electric circuit of Figure 2 that considers the passive film has defects expressed by two constant phase elements (CPE) parallel to resistances besides a serial electrolyte resistance (R_e). The software NOVA 1.11.2, with the Randomize plus Simplex methods, was used to fit the diagrams.

Analysis of variance (ANOVA) was used to determine the significance of the shape and surface quality factors of the passivation current density of the Ti-6Al-4V alloy. The results of one-way ANOVA in the average of the corrosion potential (E_{corr}) and current density (measured at 0.500 V SCE) variables. The p-value specifies the least significant level that would lead to the rejection of the null hypothesis. When the p-values are less than or equal to 0.05 (95% interval of confidence), the factors significantly affect the response model. R^2 coefficient indicates how well the variability of the observed electrochemical responses can be explained by the independent variables (shape and surface finishing). Thus, when the R^2 approaches 1, the prediction of the passivation rate is more accurate.

Darling's normality test was used to estimate the normal distribution of the residuals of the electrochemical responses.

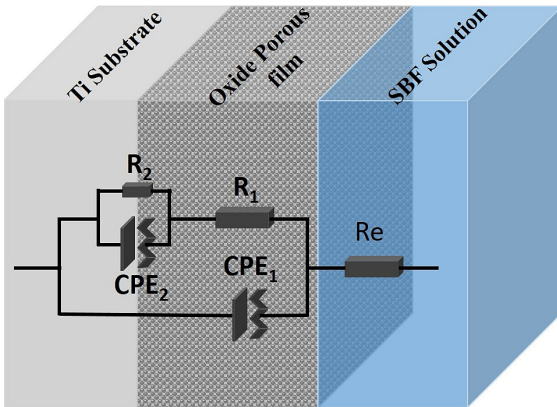


Figure 2. Equivalent circuit for EIS measurements of Ti-6Al-4V alloy tested electrochemically in SBF.

This statistical output verifies the adequacy of the model. In this case, p-values greater than 0.05 (95% interval of confidence) reveals that the residual of the E_{corr} and current density (at 0.500 V SCE) follows a normal distribution, validating the ANOVA procedure.

3. Results and Discussion

3.1. Microstructure and surface characterization

Table 2 shows the surface roughness (R_a and R_z) of the samples after the different surface finishes studied, and Figure 3a presents the microstructure after metallographic etching. The Ti-6Al-4V alloy consists of alpha α /beta β microstructure, resulting in diverse morphologies. The microstructure consists of equiaxial alpha (white phase) as matrix and spherical beta particles (black phase). The amount of the alpha phase and the morphology of the beta phase are related to the manufacturing process or heat treatment used²¹ and influenced the mechanical properties. Figure 3b depicts the XRD data that reveals the Ti-alpha hexagonal phase and a small amount of Ti-beta body-centered cubic phase.

3.2. Corrosion test for different surface finishing

Figure 4 shows the titanium alloy's anodic polarization curves for the four surface conditions (sanded up to 120, 600, #1200; and polished). The alloy showed spontaneous passivation behavior for all surface finish conditions with a passivation domain. Hence no pitting was observed in the anodic potential up to 1.5 V SCE. This behavior suggests the formation of a passive film on the surface. These results are then in line with the study of Sharma et al.¹³, which demonstrates that the oxidizing nature of the SBF solution favors a stable passive behavior. Moreover, the

Table 2. Surface roughness (R_a and R_z) of the samples after different surface preparation.

Sample condition	R_a (μm)	R_z (μm)
#120	1.37 \pm 0.03	8.77 \pm 1.86
#600	0.17 \pm 0.01	1.27 \pm 0.15
#1200	0.08 \pm 0.01	0.83 \pm 0.05
Polished	0.08 \pm 0.05	0.7 \pm 0.1

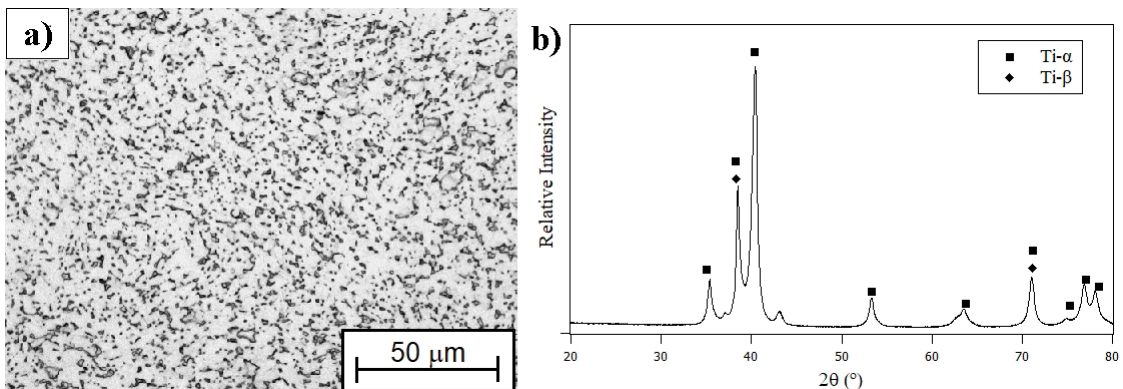


Figure 3. Microstructure (a) and XRD data to phase identification (b).

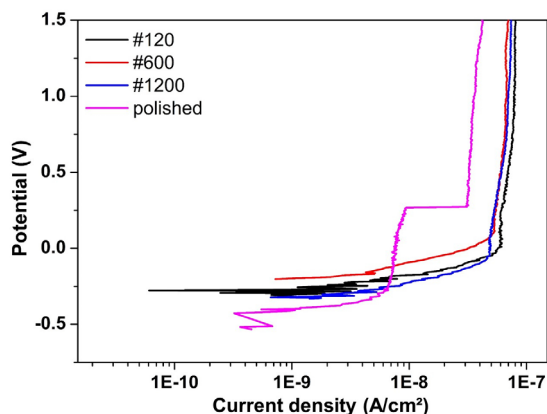


Figure 4. Anodic polarization curves in a naturally aerated SBF medium.

presence of calcium and phosphate ions in supersaturated concentration^{22,23} could improve the corrosion resistance of the samples in this environment.

As the anodic polarization indicated a passive behavior, the passive current density was evaluated at 0.500 V SCE. This potential is in the onset of the passivation range and gives the passive current density for all surface conditions. Table 3 exhibits the measured pH, the E_{corr} values, and passive current density at 0.500 V SCE for the evaluated conditions. The pH values showed negligible differences, hence the adjustment with HCl suggested by Kokubo and Takadama²⁰ was not performed.

For finishing conditions with sandpaper #120, 600, and 1200, the E_{corr} values ranged from *ca.* -0.34 to -0.21 V SCE. The polished surface showed a more negative E_{corr} value (-0.432 V SCE). However, it presented the lowest passive current density (3.23×10^{-8} A/cm²) concerning the other sanded surfaces (in the range 6.0×10^{-8} A/cm²). Moreover, the lower E_{corr} value suggesting the polished sample could present higher initial corrosion susceptibility. However, the samples with higher roughness presented higher current density, demonstrating that surface integrity influences the corrosion resistance as observed by other authors^{13,24-26}. For instance, Chi et al.²⁵ concluded that a smooth surface (polished surface) could exhibit lower corrosion potential, although it favors the passive film formed on the surface. The solution pH has no significant variation and indicates the anodic and cathodic processes are low, as expected for a passive alloy.

Figures 5 and 6 depict the diagrams of Nyquist and Bode, respectively, in the SBF solution. Table 4 shows the simulated EIS equivalent circuit parameters for different surface finishes. The capacitive semicircles observed in Figure 5 are similar for the four surface conditions, and they may be related to the passive film. Moreover, micro defects in the oxide film structure produced distorted semicircles, allowing the contact of the solution with active regions of the material. Thus, the film needs to reestablish itself on these failures²⁵. In the polished sample, the capacitive arc reached the highest values among the conditions evaluated, suggesting a greater protective capacity of the formed film and corroborating potentiodynamic polarization results

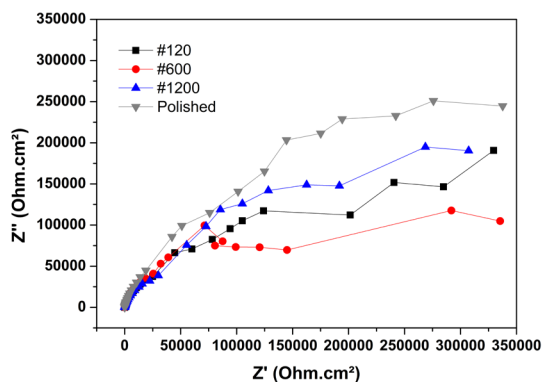


Figure 5. Nyquist diagram for Ti-6Al-4V samples with different surface finishing. Z' and Z'' are real and imaginary parts of impedance.

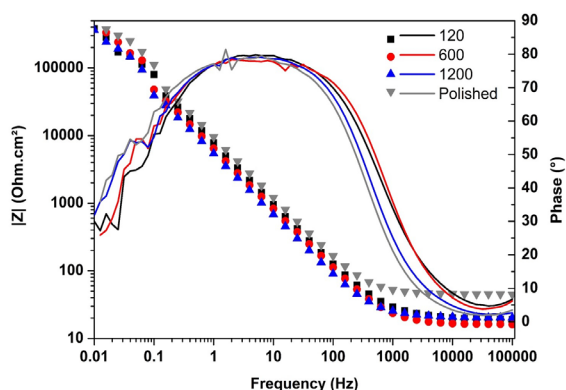


Figure 6. Bode modulus and phase diagrams of Ti-6Al-4V samples with different surface finishing immersed in SBF.

Table 3. Measured data: pH, E_{corr} , and current density at 0.500 V SCE for samples with different surface finishing. The pH was measured at 25 °C.

Surface finishing	pH	E_{corr} (V SCE)	j (A/cm ²) at 500 mV SCE
#120	7.27	-0.265	6.92×10^{-8}
#600	7.24	-0.208	6.04×10^{-8}
#1200	7.25	-0.338	6.15×10^{-8}
Polished	7.27	-0.432	3.23×10^{-8}

(Figure 3). The higher resistance observed for the polished surface at high frequency indicates more resistive film since the electrolyte is constant.

In Figure 5, there is a tendency to reduce the capacitive arc with increasing roughness. In accordance, some authors^{13,24} relate the reduction in impedance as roughness increases, with the ease of ions in the SBF solution being adsorbed on the passive film formed on the roughest surfaces, thus causing an increase in the corrosive process. Thus, the polished surface showed improvements in the protective characteristics of titanium due to the solution's difficulty in penetrating the smallest roughness pores. Furthermore,

Table 4. Simulated parameters of the EIS equivalent circuit for different surface finishing.

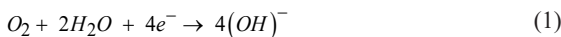
Equivalent circuit data	Surface finishing			
	#120	#600	#1200	Polished
R_c (Ohm)	19	8	20	45
R_1 (Ohm)	103341	204681	90482	139275
CPE_1 ($F_s^{(a-1)}$)	25.3×10^{-6}	29.3×10^{-6}	36.8×10^{-6}	20.2×10^{-6}
a_1	0.895	0.901	0.8932	0.8994
R_2 (Ohm)	420307	50250	385733	427090
CPE_2 ($F_s^{(a-1)}$)	26.0×10^{-6}	44.5×10^{-6}	23.4×10^{-6}	9.67×10^{-6}
a_2	1	0.976	0.8564	0.7533

the lower the roughness, the smaller is the surface area of the substrate in contact with the electrolyte^{24,25,27}. Thus, the passivation rate increases with the reduction of roughness; that is, the better the surface finish, the less the chance of reaching potential for the formation of pits²⁸.

In Figure 6, it is possible to see a small increase in impedance at low frequencies as the roughness is reduced, which could suggest an increase in corrosion resistance, mainly of the polished surface, corroborating the results of Nyquist (Figure 5) and polarization (Figure 4). Furthermore, the values for the phase angles (Figure 6) in the four samples with different roughness reached the maximum value close to 80°, which remained for a wide range of frequencies, approximately between 1 and 100 Hz. These results are in agreement with the behavior found by Chi et al. in their studies²⁵. Furthermore, according to Pieretti and Costa²⁹, the existence of high angles at low and medium frequencies is characteristic of materials that form stable passive films, in this case, proving the formation of a stable TiO₂ layer on the surfaces of the samples.

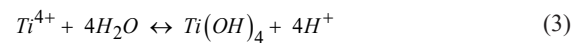
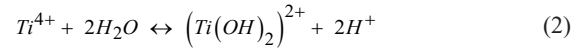
In the high-frequency region, it is possible to observe the proximity of the resistivity of all surfaces of 120, 600, #1200 and polished with the higher EIS modulus to the polished surface. In this region, the impedance modulus is practically constant; this characteristic represents the resistive behavior of the SBF solution; this result is according to the curves presented by Sharma et al.¹³. From the intermediate frequencies to the lowest frequencies, it is noted that the less rough surfaces (#1200 and polished) showed higher values for impedance. This feature indicates that the passive film is more capacitive for these surfaces.

The range in the roughness might be seen as defects with different depths, *i.e.*, #120 finishing being related to the deepest and the polished sample the shallowest. According to Gai et al.¹⁷, the crevice corrosion behavior on surfaces with pores limits the oxygen supply inside the pore since it hinders the mass transfer. Also, the pH varies at different positions and depths of pores due to the reduction of oxygen of the primary cathodic reaction in this environment.



Then, it is possible to suggest that the supply of oxygen was satisfactory for the polished samples to guarantee the

occurrence of the cathodic reaction on the surface, although in a passivation scenario. On the other hand, for conditions with higher roughness, the amount of oxygen available inside the structure was smaller than the consumption by the cathodic phenomenon. Therefore, it is expected that a delay in the cathodic kinetics might force the electrons to flow towards the region with a better supply of oxygen for the cathode process. This process might lead to a greater dissolution rate of the passive film than its formation and self-healing, increasing the amount of Ti⁴⁺. When the titanium ions reach a significant concentration, the hydrolysis reaction occurs (Equation 2 and Equation 3). The H⁺ produced leading to a decrease in the pH. Thus, it is possible to infer that this local acidification contributes to increasing the current densities of conditions with rougher finishing.

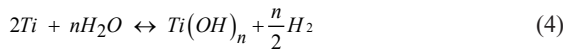


For titanium alloys, it is observed a high charge density that impedes the stabilization of Ti(OH)₄, even though the most stable oxidation state being 4+. In this case, a hydrated compound TiO₂·H₂O is expected as the final stable product. The local acidification suggested conditions with higher roughness. The high concentration of positive ions such as Ti⁴⁺ and H⁺ contributes to an increase in the flow of aggressive chloride ions towards the deeper positions on the metal surface to maintain the equilibrium of the reaction. This process aggravates the crevice mechanism in regions with low O₂ availability, increasing the passive film dissolution rates.

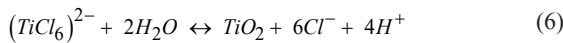
The measured corrosion potential and average pH (Table 3) can be compared with the E-pH phase diagram for the Ti-H₂O system (Figure 7). It is observed that the experimental data is inside the passivation zone of TiO₂. In Figure 7, the potential is referred to as standard hydrogen electrode - SHE, but the conversion from SCE was applied. Thus, the titanium of the alloy is more likely to passivate than to corrode for all conditions evaluated. This stability explains why the samples did not present pitting in the potentiodynamic polarization (Figure 4). Based on the Gai et al.¹⁷ findings, this indicates

that even though local electrochemical activity is intensified by surface morphology, the formation of TiO_2 is prevalent for every condition.

Rougher surfaces still presented inadequate electrochemical responses, as seen in Figures 4-6 and Table 3. Thus, Gai et al.¹⁷ suggested that, due to the effects observed in the micro-environment inside the rough surfaces, it is important to elucidate the process of passive film formation in such conditions. This mechanism is complex given the differences in the oxygen supply, and this formation will depend on local surface characteristics. For conditions with oxygen supply, the passive films form directly by the interaction between the water and titanium.



During the anodic polarization tests, an induced increase in the potential implies the growth of passive films on the alloy surface. Consequently, in regions with a plentiful supply of oxygen, the film continues to thicken throughout the test. Nevertheless, in rougher surfaces, given the increase in the chloride concentration combined with low oxygen content, Ti films are formed differently. According to the literature¹⁷, part of the passive film is formed following reaction (2), by the hydrolysis of Ti^{4+} , and also by the complex hydrolysis mechanism of $(TiCl_6)^{2-}$. The latter is formed during the degradation process of the passive film by the presence of chloride, from the combination of Ti ions with the Cl^- adsorbed on the surface replacing the O^{2-} ions. When a critical concentration of $(TiCl_6)^{2-}$ is observed, this compound is hydrolyzed to form oxides. The reactions that govern this process are:



Moreover, the degradation process in the passive film is caused by the increase in the chloride amount. Therefore, further

hydrolysis steps might repair the oxide coverage integrity of conferring again protective features. This continuous self-healing avoids the appearance of pitting corrosion in titanium alloys even under aggressive environments. This ability of the TiO_2 film to repair itself may small scattering in the polarization curve without substantial modification of steady-state values.

3.3. Shape effects on corrosion tests

Figure 8 shows the polarization curves for the different milled shapes (concave, convex, and flat) of samples immersed in the simulated body fluid at a temperature of 37 °C. The curves obtained by applying an anodic potential scan suggest forming a protective oxide film for the different shapes. Table 5 shows the values obtained from the anodic polarization curves.

Even with the corrosion potentials of concave and convex samples showing close values, more electronegative than the flat sample, the concave and convex surfaces showed a lower passivation current than the flat surface. In addition, in the potential range close to 1 V SCE, the concave sample showed a slight increase in current density, suggesting a possible instability in the passive film. The change in the shape possibly modified the active area of the sample, which can generate different rates of corrosion as discussed in the literature²⁹⁻³². As the density of anodic current was lower for concave and convex surfaces (Table 4), possibly the corrosion rate will be lower on these surfaces. Several authors³¹⁻³³ reported that in vivo and in vitro studies, the surface topography affects the biological functions of cells, contributing to the repair and regeneration of bone cells³⁴. The machining produces residual stresses with higher

Table 5. Measured pH, E_{corr} , and current density 0.500 V SCE for samples with different shapes. The pH was measured at 25 °C.

Sample shape	pH	E_{corr} (V SCE)	j (A/cm^2) at 0.500 V SCE
Concave	7.22	-0.357	3.07×10^{-8}
Convex	7.21	-0.383	5.59×10^{-8}
Flat	7.24	-0.203	6.49×10^{-8}

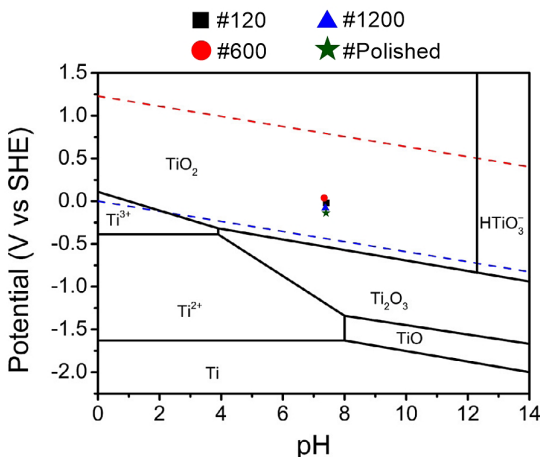


Figure 7. E-pH phase diagram for $Ti-H_2O$ system (TiO_2 and Ti_2O_3 are in the hydrated state). Adapted from Gai et al.¹⁷.

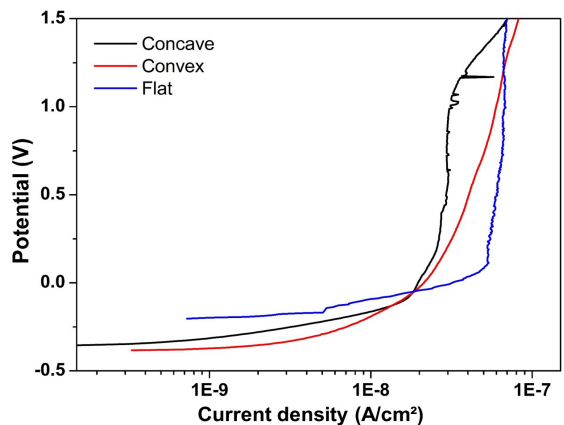


Figure 8. Polarization curves in SBF, naturally aerated, for Ti-6Al-4V with different shapes.

levels on the surface, and the passive film could be affected, reflecting on the electrochemical response.

Although the concave surface presented lower current density than the convex surface (Table 3), it presented a process of increasing anodic current density at anodic potential of 1.2 V, characterized as pite potential (Figure 8). It is also possible to verify in Figure 8 that the concave surface presents small disturbances of increased current density in applied anodic potentials, which may probably be associated with breakage in the passive film and onset of pitting corrosion. However, it was not observed for convex and flat samples, where the occurrence of pite potential was not verified. Consequently, the concave samples presented a lower electrochemical behavior in relation to the other surface preparation conditions.

Figure 9 presents the Nyquist diagram of impedance in SBF solution for the three shapes evaluated here. It can be noticed the presence of only one semicircle for the flat and convex shapes, characteristic of a capacitive film. This diagram is related to the film capacitance on the surface, which can present microcracks and minor defects, allowing the substrate/solution contact as described in the reference²⁵. On the other hand, for the concave surface, which presented the worst electrochemical behavior, it is possible to notice at low frequency the onset of another arc, presenting capacitive behavior, suggesting more than one time constant.

The loop formed in the lower frequencies is associated, probably, to slow process as film evolution or diffusion events, while the high-frequency loop is related to the passive film although not completely perfect, as described in other studies^{25,35}. This behavior suggests that the convex surface, which presents the highest capacitive loop, allowed the most stable and protective film to form and with the lowest number of defects. These results are in accordance with the polarization data, whose continuous potential increases with time and favors passive film formation. Thus, it is possible to observed that different shapes affect the distribution of potential and current density, as reported elsewhere^{32,36}.

According to McMurray et al.¹⁶, a convex-shaped sample, in addition to favoring the presence of pores, also favors the O₂ diffusion on its surface. This assumption validates the results shown in Figure 8 and Figure 9, in which the convex sample suggests the higher formation of Ti oxides films,

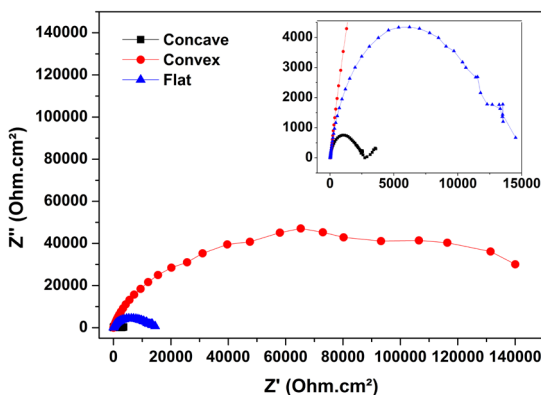


Figure 9. Nyquist diagram of samples with different shape.

following the reactions proposed by Gai et al.¹⁷. For the authors, convex regions tend to be strongly cathodic, and anodic reactions occur preferentially in the concave regions. Thus, the shape of the surface significantly influences the distribution of electrochemical activity on the sample surface.

This fact occurs because the convex surface favors the contact of oxygen atoms with the active regions of the surface, favoring the formation reactions of Ti oxides. On the other hand, the concave surface hinders the dissolution of the species through the diffusion layer, hindering the formation reactions and impairing the protective capacity of the oxide film formed. Consequently, the concave samples showed the worst electrochemical behavior in anodic polarization curves and electrochemical impedance.

Martínez et al.³⁶ showed in their results a strong effect of shape on the impedance results, especially in the high to intermediate frequency regions. With an increase in the phase angles. This phenomenon can arise due to a frequency dispersion due to the effect of the electrode shape that can favor or hinder the distribution of currents over the electrode surface.

For concave surfaces, the directions normal to the surfaces intersect, generating a non-uniformity of currents and time constants, consequently, generating a worsening in the electrochemical responses.

Figure 10 shows the Bode diagrams for the different shapes. In the region with the highest frequency (above *ca.* 10 kHz), it is possible to observe a similarity in the resistance of all shapes until the modulus is practically constant. Regarding the regions of intermediate frequency to low frequencies, as the regions closest to the metal/electrolyte interface are evaluated, an increase in the impedance modulus is observed for all surfaces. However, the convex surface showed higher values for Z, indicating a greater protective capacity of the formed film.

The quantitative parameters of the simulated equivalent circuit for the 3 different shapes are shown in Table 6.

CPE results are related to films' capacitive/protective characteristics formed on the surface^{26,34}. The phase angles shown in Figure 8 suggest that the milled surface with a convex shape presents a more capacitive behavior, with phase angle values close to 75° and extending over a greater frequency range (~ 0.1 to 100 Hz). On the other hand, the

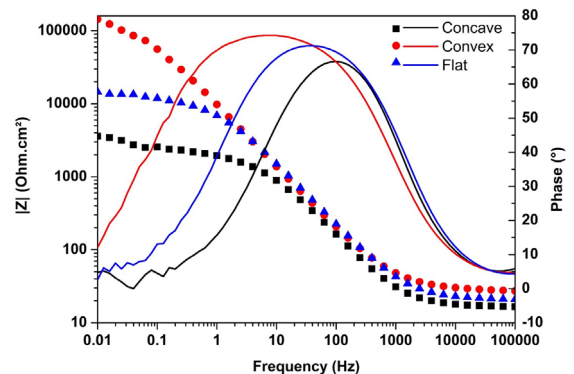


Figure 10. Bode modulus and phase diagrams for the Ti-6Al-4V alloy electrode immersed in SBF for the different shapes (concave, convex and flat).

flat sample presented maximum phase angle values around 70° and remained for approximately a decade of frequency. Corroborating with the results of Figure 8, the concave surface presented the lowest value of phase angle ($\sim 65^\circ$) and a narrow frequency range. Moreover, below 0.5 Hz, the phase reveals a scattering not correctly seen in Nyquist format. The worst behavior in the EIE tests on the concave surface may be related to the instability in the current density values obtained at potentials around 1 V SCE in the polarization tests of Figure 7. Thus, even with the concave surface presenting a lower current density, the concave sample can have formed a film with a very low a_2 CPE exponent not related to a perfect passive behavior of films.

The equivalent circuit was used to adjust the EIE results to evaluate the corrosion mechanisms that occurred at the Ti-6Al-4V/electrolyte (SBF) interface. This circuit is composed of two CPEs is used by several authors in the literature to explain the electrochemical responses of titanium alloys^{13,37,38}. Then, for the Ti-6Al-4V alloy, the equivalent circuit is composed of resistance of the test solution (R_e); capacitance of the Ti-6Al-4V substrate surface, being a constant phase element (CPE_1); resistance to charge transfer at the Ti-6Al-4V/electrolyte interface, in the outer layer of the material associated with some areas of the surface that have ionic conduction, called porous resistance (R_1); the elements R_2 and CPE_2 represent the resistance to charge transfer and the capacitance of the passive film interface with the Ti-6Al-4V substrate surface, that is, the inner layer of the passive film on the material surface.

At high frequencies, the impedance of Ti-6Al-4V samples has a dominant ohmic behavior, being controlled by the electrolyte resistance (R_e). At intermediate frequencies, the system is controlled by the capacitance of the alloy (CPE_1) and the resistance to load transfer at the Ti-6Al-4V/electrolyte interface (R_1). In addition, at low frequencies (10^{-3} to 10^{-1} Hz), the impedance is mainly affected by the resistance (R_2) and the element (CPE_2), related to the interface of the inner layer of the passive film and the Ti-6Al-4V substrate. These results agree with the literature³⁷, where it is a consensus that in an SBF solution, this titanium alloy presents capacitive behavior related to the film, frequently porous, besides the oxides formed on the surface.

The long passivation potential zone, along with the electrochemical data for different surface textures, demonstrated that a passive layer could form on the titanium alloy, regardless of the surface characteristics. This fact suggests good condition to bone-metal interaction in SBF medium. As regards osseointegration and cellular adhesion, the biocompatibility process is a function of cell contact and proliferation with the implant surface. Consequently, in this system, the prosthesis material characteristics, such as shape and surface roughness, could play an essential role in the cell adhesion of orthopedics/dental implants. According to the literature, the most determining surface characteristics for cell adhesion are surface topography, surface texture, or surface reactivity²⁻⁴.

The analysis of variance (Table 7) reveals that shape and emery paper granulometry have a significant influence (p -value < 0.05) on the electrochemical parameters of Ti-6Al-4V in SBF. Figure 11 shows the main effect plots.

Table 6. Simulated parameters of the EIS equivalent circuit for different sample shapes.

Equivalent circuit data	Shape		
	Concave	Convex	Flat
R_e (Ohm)	16	28	21
R_1 (Ohm)	1801	125233	11184
CPE_1 (F.s ^(a-1))	25.17×10^{-6}	21.55×10^{-6}	19.75×10^{-6}
a_1	0.8538	0.8419	0.8419
R_2 (Ohm)	1437	75580	2877
CPE_2 (F.s ^(a-1))	8.073×10^{-4}	7.469×10^{-5}	5.419×10^{-4}
a_2	0.473	0.9977	0.7769

Table 7. One-way ANOVA test.

Factor	Ecorr	j at 500 mV SCE
	p-value	p-value
Surface finishing	0.000	0.027
R² (adj)	0.9861	0.8779
Darling	0.523	0.913
Factor	Ecorr	j at 500 mV SCE
	p-value	p-value
Surface shape	0.015	0.001
R²	0.899	0.8788
Darling	0.552	0.245

Passivation rate studies in simulated human environments allow us to understand the corrosion process, as shown in the related literature³⁹⁻⁴². Irrespective of the type of surface shape of titanium implants, the nature of the surface film, which interacts with cells and bone, provides enhanced cellular and biocompatibility mechanisms. Rupp et al.⁴³ showed pieces of evidence that suitable surface roughness, at nano and microscale, can lead to successful osseointegration of titanium implants.

In general, surface finishing is a good predictor of how the mechanical component will interact with the physiological environment. For example, adequate roughness may improve cellular adhesion or optimize a surface's dental and orthopedic implants⁴⁴. In the present study, the corrosion potential turns more negative when the surface prepared with #120 abrasive (-265 mV) changes to the polished surface (-432 mV) (see Figure 11a). However, the reduction in the passive current density at 500 mV SCE with the smooth surfaces (Figure 11c) is more significant. In this way, surface finishing preparation exhibits a considerable contribution to the formation of oxide film, in which the passivation current density is lower for the polished surface.

When the shape effect on E_{corr} (Figure 11b) is analyzed, it is noticed that the concave surface and the convex presents similar values. The more significant influence was on the flat surface (-403 mV), which demonstrated a smaller tendency for the corrosive mechanisms. This fact implies that surface topography could be a fundamental parameter used to define cell behavior. The initial contact of the engineered surface with biological tissues, the cell-topographical interactions will significantly influence the cell attachment and osseointegration

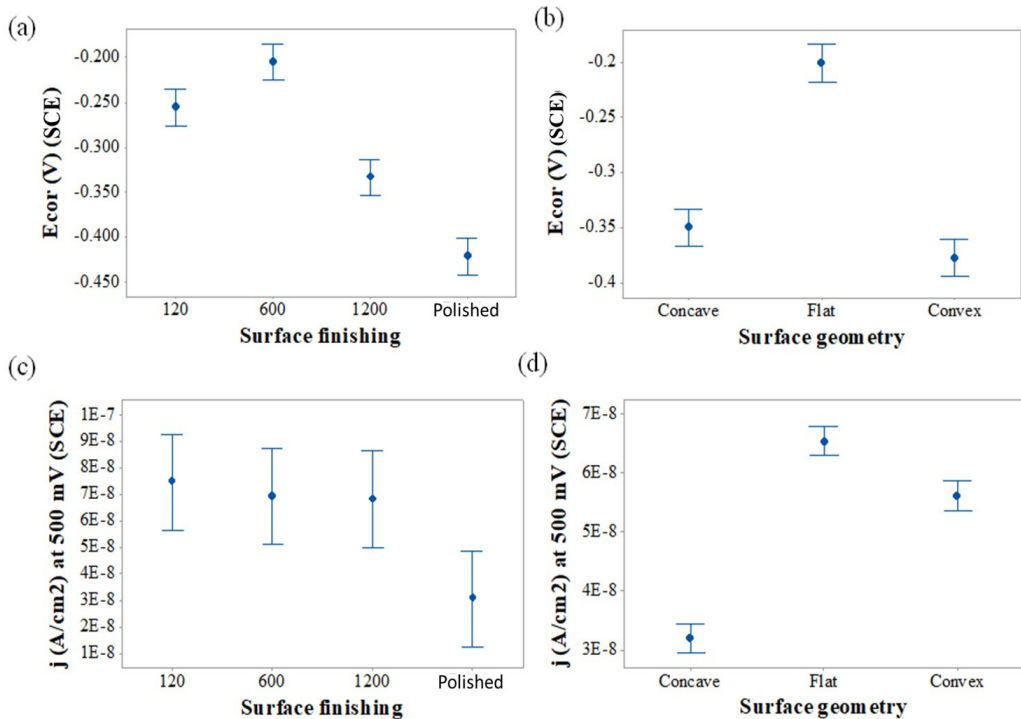


Figure 11. Main effect plots related to electrochemical data.

of the implants⁴⁵. Ogawa et al.⁴⁶ reported that the surface texture could induce phenotypic cell alteration during healing. Elias et al.⁴⁷ also found this tendency and concluded that this phenomenon is related to the differentiation of bone cell formation. Finally⁴⁸⁻⁵⁴, affirmed that the surface topography directly influences the biological responses as cellular production and migration.

4. Conclusions

The corrosion resistance of Ti-6Al-4V alloy in a simulated body fluid (SBF) was studied here, evaluating the influence of surface roughness and geometry. Independently of roughness or geometry, the passivity was observed in polarization tests, characteristic of Ti6Al4V tested in SBF. The roughness characteristics presented some influence, with smooth surfaces (polished) presenting better results in polarization and impedance tests. Regarding the different geometry, the effects of shape and geometry are often not taken into account in corrosion studies. However, the results showed that there is an effect that must be observed, being important for implant and prosthesis manufacturing, it was demonstrated that concave shapes are more susceptible to corrosion than convex ones because of the occurrence of pitting potential on the anodic polarization curve. This result is in opposition to the biological responses found in the literature, where concave surfaces are better for cells growth, suggesting that medical devices product developers should pay attention to these geometrical characteristics. As future studies, the influence of concavity/convexity level could bring interesting information for prosthesis/implants designers, and biological tests in vitro and/or in vivo should

be performed to evaluate if these geometric differences can influence osteointegration.

5. Acknowledgments

The authors would like to acknowledge FAPEMIG and CNPq for the financial research support. This study was financed in part by the Coordenação de Aperfeiçoamento de Pessoal de Nível Superior – Brasil (CAPES) – Finance Code 001.

6. References

1. Tathe A, Ghodke M, Nikalje AP. A brief review: biomaterials and their application. *Int J Pharm Pharm Sci.* 2010;2:19-23.
2. Hasirci V, Hasirci N. *Fundamentals of biomaterials.* New York: Springer; 2018. Tissue-biomaterial interactions; p. 141-57. <https://doi.org/10.1007/978-1-4939-8856-3>.
3. Izman S, Abdul Kadir M, Anwar DM, Nazim EM, Rosliza R, Shah A, et al. Surface modification techniques for biomedical grade of titanium alloys: oxidation, carburization and ion implantation processes. In: Nurul Amin AKM, editor. *Titanium alloys - towards achieving enhanced properties for diversified applications.* London: IntechOpen; 2012. <https://doi.org/10.5772/36318>.
4. Asri RIM, Harun WSW, Samykano M, Lah NAC, Ghani SAC, Tarlochan F, et al. Corrosion and surface modification on biocompatible metals: a review. *Mater Sci Eng C.* 2017;77:1261-74. <http://dx.doi.org/10.1016/j.msec.2017.04.102>.
5. Zhang LC, Chen LY. A review on biomedical titanium alloys: recent progress and prospect. *Adv Eng Mater.* 2019;21:1-29. <http://dx.doi.org/10.1002/adem.201801215>.
6. Geetha M, Singh AK, Asokamani R, Gogia AK. Ti based biomaterials, the ultimate choice for orthopaedic implants -

- A review. *Prog Mater Sci.* 2009;54:397-425. <http://dx.doi.org/10.1016/j.pmatsci.2008.06.004>.
7. Kaur M, Singh K. Review on titanium and titanium based alloys as biomaterials for orthopaedic applications. *Mater Sci Eng C.* 2019;102:844-62. <http://dx.doi.org/10.1016/j.msec.2019.04.064>.
 8. Sidambe AT. Biocompatibility of advanced manufactured titanium implants-A review. *Materials (Basel).* 2014;7:8168-88. <http://dx.doi.org/10.3390/ma7128168>.
 9. Yue TM, Yu JK, Mei Z, Man HC. Excimer laser surface treatment of Ti – 6Al – 4V alloy for corrosion resistance enhancement. *Mater Lett.* 2002;52:206-12. [http://dx.doi.org/10.1016/S0167-577X\(01\)00395-0](http://dx.doi.org/10.1016/S0167-577X(01)00395-0).
 10. Eisenbarth E, Velten D, Muller M, Thull R, Breme J. Biocompatibility of β -stabilizing elements of titanium alloys. *Biomaterials.* 2004;25(26):5705-13. <https://doi.org/10.1016/j.biomaterials.2004.01.021>.
 11. William F. Carcinogenicity of metal alloys in orthopedic prostheses. *Clinical and Experimental Studies.* 1989;16:205-16.
 12. Manam NS, Harun WSW, Shri DNA, Ghani SAC, Kurniawan T, Ismail MH, et al. Study of corrosion in biocompatible metals for implants: a review. *J Alloys Compd.* 2017;701:698-715. <http://dx.doi.org/10.1016/j.jallcom.2017.01.196>.
 13. Sharma A, Oh MC, Kim JT, Srivastava AK, Ahn B. Investigation of electrochemical corrosion behavior of additive manufactured Ti–6Al–4V alloy for medical implants in different electrolytes. *J Alloys Compd.* 2020;830:154620. <http://dx.doi.org/10.1016/j.jallcom.2020.154620>.
 14. Cheng X, Roscoe SG. Influence of surface polishing on the electrochemical behavior of titanium. *Electrochem Solid-State Lett.* 2005;8:B38. <http://dx.doi.org/10.1149/1.1996509>.
 15. Walley KC, Bajraliu M, Gonzalez T, Nazarian A. The chronicle of a stainless steel orthopaedic implant. *Orthop J Harvard Med Sch.* 2016;17:68-74.
 16. McMurray HN, Searle J, Wilson B. The use of SVET for investigating changes in the corrosion mechanism induced by forming galvanised steel samples, *EuroCorr* 2000; 2000; London. London: Queen Mary and Westfield College; 2000.
 17. Gai X, Bai Y, Li S, Hou W, Hao Y, Zhang X, et al. In-situ monitoring of the electrochemical behavior of cellular structured biomedical Ti-6Al-4V alloy fabricated by electron beam melting in simulated physiological fluid. *Acta Biomater.* 2020;106:387-95. <http://dx.doi.org/10.1016/j.actbio.2020.02.008>.
 18. Zadpoor AA. Bone tissue regeneration: the role of scaffold geometry. *Biomater Sci.* 2015;3:231-45. <http://dx.doi.org/10.1039/c4bm00291a>.
 19. ASTM International. ASTM G5-94(2011), Standard Reference Test Method for Making Potentiostatic and Potentiodynamic Anodic Polarization Measurements. West Conshohocken, PA: ASTM International; 2011. <https://doi.org/10.1520/G0005-94R11E01>.
 20. Kokubo T, Takadama H. How useful is SBF in predicting in vivo bone bioactivity? *Biomaterials.* 2006;27:2907-15. <http://dx.doi.org/10.1016/j.biomaterials.2006.01.017>.
 21. Donachie MJ Jr. 2000. Titanium: a technical guide. Materials Park, OH: ASM International.
 22. Alves VA, Reis RQ, Santos ICB, Souza DGT, Pereira-da-Silva MA, Rossi A, et al. In situ impedance spectroscopy study of the electrochemical corrosion of Ti and Ti-6Al-4V in simulated body fluid at 25 °C and 37 °C. *Corros Sci.* 2009;51:2473-82. <http://dx.doi.org/10.1016/j.corsci.2009.06.035>.
 23. Bastos IN, Platt GM, Andrade MC, Soares GD. Theoretical study of Tris and Bistris effects on simulated body fluids. *J Mol Liq.* 2008;139:121-30. <http://dx.doi.org/10.1016/j.molliq.2007.12.003>.
 24. Nakatani M, Masuo H, Tanaka Y, Murakami Y. Effect of surface roughness on fatigue strength of Ti-6Al-4V alloy manufactured by additive manufacturing. *Procedia Struct Integr.* 2019;19:294-301. <http://dx.doi.org/10.1016/j.prostr.2019.12.032>.
 25. Chi G, Yi D, Liu H. Effect of roughness on electrochemical and pitting corrosion of Ti-6Al-4V alloy in 12 wt.% HCl solution at 35 °C. *J Mater Res Technol.* 2019;9:1162-74. <http://dx.doi.org/10.1016/j.jmrt.2019.11.044>.
 26. Kim SK, Park IJ, Lee DY, Kim JG. Influence of surface roughness on the electrochemical behavior of carbon steel. *J Appl Electrochem.* 2013;507-14. <https://doi.org/10.1007/s10800-013-0534-5>.
 27. Yopez OJ. Study on the effect of surface finish on corrosion of carbon steel in CO2 environment revisited. *Meet Abstr.* 2017;MA2017-01:983. <https://doi.org/10.1149/ma2017-01/15/983>.
 28. Moayed MH, Laycock NJ, Newman RC. Dependence of the critical pitting temperature on surface roughness. *Corros Sci.* 2003;45:1203-16. [http://dx.doi.org/10.1016/S0010-938X\(02\)00215-9](http://dx.doi.org/10.1016/S0010-938X(02)00215-9).
 29. Pieretti EF, Costa I. Surface characterisation of ASTM F139 stainless steel marked by laser and mechanical techniques. *Electrochim Acta.* 2013;114:838-43. <http://dx.doi.org/10.1016/j.electacta.2013.05.101>.
 30. Barranco V, Escudero ML, García-Alonso MC. Influence of the microstructure and topography on the barrier properties of oxide scales generated on blasted Ti-6Al-4V surfaces. *Acta Biomater.* 2011;7:2716-25. <http://dx.doi.org/10.1016/j.actbio.2011.02.040>.
 31. Postiglione L, Di Domenico G, Ramaglia L, Montagnani S, Salzano S, Di Meglio F, et al. Behavior of SaOS-2 cells cultured on different titanium surfaces. *J Dent Res.* 2003;82:692-6. <http://dx.doi.org/10.1177/154405910308200907>.
 32. Xu Y, Li Z, Zhang G, Wang G, Zeng Z, Wang C, et al. Electrochemical corrosion and anisotropic tribological properties of bioinspired hierarchical morphologies on Ti-6Al-4V fabricated by laser texturing. *Tribol Int.* 2019;134:352-64. <http://dx.doi.org/10.1016/j.triboint.2019.01.040>.
 33. Mironov S, Sato YS, Kokawa H. Friction-stir welding and processing of Ti-6Al-4V titanium alloy: a review. *J Mater Sci Technol.* 2018;34:58-72. <http://dx.doi.org/10.1016/j.jmst.2017.10.018>.
 34. Puleo DA, Nanci A. Understanding and controlling the bone-implant interface. *Biomaterials.* 1999;20:2311-21. [http://dx.doi.org/10.1016/S0142-9612\(99\)00160-X](http://dx.doi.org/10.1016/S0142-9612(99)00160-X).
 35. Chen X, Shah K, Dong S, Peterson L, Callagon La Plante E, Sant G. Elucidating the corrosion-related degradation mechanisms of a Ti-6Al-4V dental implant. *Dent Mater.* 2020;36:431-41. <http://dx.doi.org/10.1016/j.dental.2020.01.008>.
 36. Martínez C, Guerra C, Silva D, Cubillos M, Briones F, Muñoz L, et al. Effect of porosity on mechanical and electrochemical properties of Ti-6Al-4V alloy. *Electrochim Acta.* 2020;338:135858. <http://dx.doi.org/10.1016/j.electacta.2020.135858>.
 37. Benea L, Celis JP. Reactivity of porous titanium oxide film and chitosan layer electrochemically formed on Ti-6Al-4V alloy in biological solution. *Surf Coat Tech.* 2018;354:145-52. <http://dx.doi.org/10.1016/j.surfcoat.2018.09.015>.
 38. Bahi R, Nouveau C, Beliardouh NE, Ramoul CE, Meddah S, Ghelloudj O. Surface performances of Ti-6Al-4V substrates coated PVD multilayered films in biological environments. *Surf Coat Tech.* 2020;385:125412. <http://dx.doi.org/10.1016/j.surfcoat.2020.125412>.
 39. Ribeiro SLMFo, Lauro CH, Bueno AHS, Brandão LC. Influence cutting parameters on the surface quality and corrosion behavior of Ti-6Al-4V alloy in synthetic body environment (SBF) using Response Surface Method. *Measurement.* 2016;88:223-37. <http://dx.doi.org/10.1016/j.measurement.2016.03.047>.
 40. Gurappa I. Characterization of different materials for corrosion resistance under simulated body fluid conditions. *Mater Charact.* 2002;49:73-9. <http://dx.doi.org/10.1002/jor.23150>.
 41. Xu L, Zhang E, Yin D, Zeng S, Yang K. In vitro corrosion behaviour of Mg alloys in a phosphate buffered solution for bone

- implant application. *J Mater Sci Mater Med*. 2008;19:1017-25. <http://dx.doi.org/10.1007/s10856-007-3219-y>.
42. Cheng Z, Lian J, Hui Y, Li G. Biocompatible DCPD coating formed on az91d magnesium alloy by chemical deposition and its corrosion behaviors in SBF. *J Bionics Eng*. 2014;11:610-9. [http://dx.doi.org/10.1016/S1672-6529\(14\)60072-X](http://dx.doi.org/10.1016/S1672-6529(14)60072-X).
 43. Rupp F, Scheideler L, Rehbein D, Axmann D, Geis-Gerstorfer J. Roughness induced dynamic changes of wettability of acid etched titanium implant modifications. *Biomaterials*. 2004;25:1429-38. <http://dx.doi.org/10.1016/j.biomaterials.2003.08.015>.
 44. Hatamleh MM, Wu X, Alnazzawi A, Watson J, Watts D. Surface characteristics and biocompatibility of cranioplasty titanium implants following different surface treatments. *Dent Mater*. 2018;34:676-83. <http://dx.doi.org/10.1016/j.dental.2018.01.016>.
 45. Assender H, Bliznyuk V, Porfyraakis K. How surface topography relates to materials' properties. *Science*. 2002;297(5583):973-6. <http://dx.doi.org/10.1126/science.1074955>.
 46. Ogawa T, Sukotjo C, Nishimura I. Modulated bone matrix-related gene expression is associated with differences in interfacial strength of different implant surface roughness. *J Prosthodont*. 2002;11:241-7. <http://dx.doi.org/10.1053/jpro.2002.129772>.
 47. Elias CN, Oshida Y, Lima JHC, Muller CA. Relationship between surface properties (roughness, wettability and morphology) of titanium and dental implant removal torque. *J Mech Behav Biomed Mater*. 2008;1:234-42. <http://dx.doi.org/10.1016/j.jmbbm.2007.12.002>.
 48. Flemming RG, Murphy CJ, Abrams GA, Goodman SL, Nealey PF. Effects of synthetic micro- and nano-structured surfaces on cell behavior. *Biomaterials*. 1999;20:573-88. [http://dx.doi.org/10.1016/S0142-9612\(98\)00209-9](http://dx.doi.org/10.1016/S0142-9612(98)00209-9).
 49. Antolak-Dudka A, Płatek P, Durejko T, Baranowski P, Małachowski J, Sarzyński M, et al. Static and dynamic loading behavior of Ti6Al4V honeycomb structures manufactured by Laser Engineered Net Shaping (LENSTM) technology. *Materials (Basel)*. 2019;12. <http://dx.doi.org/10.3390/ma12081225>.
 50. Szafrńska A, Antolak-Dudka A, Baranowski P, Bogusz P, Zasada D, Małachowski J, et al. Identification of mechanical properties for titanium alloy Ti-6Al-4V produced using LENS technology. *Materials (Basel)*. 2019;16. <http://dx.doi.org/10.3390/ma12060886>.
 51. Eliaz N. Corrosion of metallic biomaterials: a review. *Mater (Basel, Switzerland)*. 2019;12:407. <http://dx.doi.org/10.3390/ma12030407>.
 52. Maestro CAR, Bueno AHS, de Sousa Malafaia AM. Cyclic thermal oxidation evaluation to improve Ti6Al4V surface in applications as biomaterial. *J Mater Eng Perform*. 2019;28:4991-7. <http://dx.doi.org/10.1007/s11665-019-04220-x>.
 53. de Almeida Bino MC, Eurídice WA, Gelamo RV, Leite NB, da Silva MV, de Siervo A, et al. Structural and morphological characterization of Ti₆Al₄V alloy surface functionalization based on Nb₂O₅ thin film for biomedical applications. *Appl Surf Sci*. 2021;557:149739. <http://dx.doi.org/10.1016/j.apsusc.2021.149739>.
 54. Maestro CAR, Ferreira MC, Bueno AHS, de Sousa Malafaia AM. Corrosion resistance of ti-6al-4v machined surfaces improved by thermal oxidation. *Eng J (NY)*. 2020;24:185-93. <http://dx.doi.org/10.4186/ej.2020.24.5.185>.